AIAA2001-4137

Static and Dynamic Wind Tunnel Testing of Air Vehicles In Close Proximity

David R. Gingras
J.L. Player

Bihrle Applied Research Inc.
Hampton, VA

William B. Blake

Air Force Research Laboratory
Wright Patterson AFB, OH

Atmospheric Flight Mechanics Conference & Exhibit
In Association with the Canadian Aeronautics and Space Institute
6 - 9 Aug 2001
Montreal, Quebec, Canada

STATIC AND DYNAMIC WIND TUNNEL TESTING OF AIR VEHICLES IN CLOSE PROXIMITY

DAVID R. GINGRAS[*] AND J. L. PLAYER[†]

Bihrle Applied Research Inc.
18 Research Drive
Hampton, VA 23666 USA
(757) 766-2416 FAX (757)766-922

WILLIAM B. BLAKE[‡]

Air Force Research Laboratory
Wright Patterson AFB OH 45433-7531

Abstract

Bihrle Applied Research Inc. has developed unique capabilities for investigating the aerodynamic effects on aircraft in close formation. Wind-tunnel experiments were conducted at the Langley Full-Scale Tunnel using special hardware and computer equipment developed specifically for formation testing. It was demonstrated that static and dynamic force and moment data, as well as surface pressure data and wake survey data, can be acquired and utilized to analyze and model vehicle in close formation flight. The data acquired is well suited for use in flight vehicle simulation for development of control laws for automated formation flight and automated refueling.

Unique to this wind tunnel testing was the simultaneously collection of force and moment data from two separate models positioned differently during each run. Also unique was the dynamic testing conducted to determine the control surface deflections required to trim the trail vehicle in various formation positions.

Introduction

There have been several theoretical and experimental studies suggesting that aircraft flying in close proximity experience performance benefits in the form of increased L/D [1,2,3]. As a result, close formation flight is being discussed for use with transports, fighters, and conceptual uninhabited combat aerial vehicles (UCAV).

Unfortunately, the performance benefit does not come without a cost. It has been shown that the aerodynamic forces and moments generated by the wake of a lead vehicle can adversely affect trail vehicle flying qualities, creating a challenging control situation [4]. To make close formation flight practical, control-law designers must be provided with representative aerodynamics models of the formation flight situation to ensure the system robustness required for tasks such as station keeping, collision avoidance, and automated aerial refueling.

Through Small Business Innovative Research effort AF98-175, Bihrle Applied Research Incorporated (BAR) has successfully conducted a series of wind-tunnel tests investigating the effects of close formation on the aerodynamic characteristics of several aircraft configurations. This paper provides details pertaining to the development and conduct of this series of wind-tunnel tests and presents examples of various test results.

Nomenclature

b	Span (ft)
CD	Drag coefficient (+aft parallel to free stream)
CL	Lift coefficient (+up normal to free stream)
Cl	Rolling moment coefficient (+right wing down)
Cm	Pitching moment coefficient (+nose up)
Cn	Yawing moment coefficient (+nose right)
CY	Sideforce coefficient (+right)
DX,X	Longitudinal distance of lead aircraft from trail aircraft (+ forward)
DY,Y	Span-wise distance of lead aircraft from trail aircraft (+ left)
DZ,Z	Vertical distance of lead aircraft from trial trail aircraft (+ down)
α	Angle of attack (deg)
β	Angle of sideslip (deg)

---

[*] Chief Test Engineer, Senior Member AIAA
† Aerospace Engineer
‡ Aerospace Engineer, Associate Fellow AIAA

Wind-Tunnel Tests

In general, formation wind tunnel testing involves mounting multiple scale models in a wind tunnel test section, moving the models into various different relative positions, and measuring the resulting aerodynamic interactions through strain-gauge balances and pressure sensing equipment. The goal of this type of testing is to determine the formation positions and aircraft conditions that maximize performance benefits (L/D increases) while minimizing force and moments that make precise station keeping difficult. Another goal is to determine the control power required to enter, exit, and remain in beneficial formation positions.

Facility

Tests were conducted at the Langley Full-Scale Tunnel, which was operated by Old Dominion University. This facility was ideal for formation testing due to the large open test section and the existing model support hardware.

The tunnel test section is nominally 30-ft. high and 60-ft. wide, with a quasi-elliptical cross-section. It is a closed circuit, three-quarter open-jet, double-return, continuous flow design which operates at atmospheric pressure. The airflow from the dual fans mounted within the collector cone is split right and left into two equal streams, each doubling back between the test section and the building walls to the entrance cone, reuniting prior to the contraction section upstream of the test section. The tunnel is powered by two 4,000-hp electric motors, each driving a four-blade 35.5-ft laminated wood propeller. The motors are mounted with rotor shafts centered within the exit cone passages [5].

The test section is equipped with a main model support. Located on the test section centerline, it is capable of angle-of-attack and angle-of-sideslip changes. The tunnel also features an overhead carriage that has been used for flow surveys and is capable of translating in three directions within the test section, both horizontally, vertically, and along the freestream. Both the carriage and main support can be seen in Figure 1.

Apparatus

Test hardware was fabricated and installed to allow for the independent measurement of force and moment data from both the lead vehicle and trail vehicle and to allow for the trail vehicle to be moved in and out of various formation positions.

A test apparatus was designed for the survey carriage to provide a balance mount capable angle-of-attack changes. This mount allowed the model to be pitched ± 25 degrees relative to the tunnel freestream as seen in Figure 2.

An adapter was also built for the main model support allowing the model to translate to maintain constant vertical position with changes in angle-of-attack. This rig also enabled the model to translate in and out of a specific formation position as illustrated seen in Figure 3.

Data Acquisition

During testing, four types of data were acquired. These included, static and dynamic force and moment data, surface pressure data, and wake survey data. Each type was acquired using a data acquisition computer (DAC) specifically built by BAR to establish multi-vehicle test capability.

Installed on the DAC was BAR's wind-tunnel data acquisition software which is capable of reducing static and several types of dynamic force and moment data, as well as surface pressure data. Also installed was BAR's D-Six™ Simulation software and associated Input / Output Module which allows acquired digital signals to be acquired, mapped to simulation variables, and manipulated.

The DAC contained a Pentium II processor running at 233 megahertz with 128 megabytes of RAM and a four-gigabyte hard drive. The DAC was equipped with a Trans Era Model 650 16bit GPIO interface card for communications with both a NEFF 620 Analog-to-Digital Converter and a PSI Model 780B ESP (Electronically Scanned Pressure) Controller. The DAC also featured a National Instruments Data Acquisition Card (NIDAQ) for communication with the D-Six I/O Module.

Test Procedure

In each of the test entries, a number of test parameters was set including relative distance between lead and trail vehicle, angle-of-attack of each vehicle, angle-of-sideslip of each vehicle, and model control surface deflections. At each test condition, force and moment data was collected from both the lead and trail models simultaneously. Static force and moment was reduced by time-averaging 20 seconds of data sampled at 25 Hz from twin SPT-2 six-component strain gauge balances. During dynamic tests, balance signals were sampled at 25 Hz and were stored directly.

Surface pressure data was collected from a single featuring over 256 static ports connected to several internally mounted ESP modules (0.35 PSI rated). Differential pressures at each port were sampled at 10 Hz and were time averaged, reduced to coefficient form, stored, and then visualized used BAR's Reveal™ software. Wake survey data was obtained using a five-

hole probe mounted to the carriage rig and connected to an ESP module.

Unique to this investigation was the series of dynamic tests designed to determine control surface deflections required for maintaining trimmed flight while in close proximity to other aircraft. To accomplish this, a trim algorithm utilizing an integral controller was written in C++ and implemented in D-Six™. The control is diagrammed in Figure 4.

Using the D-Six™ Input / Output module and NIDAQ card interface, balance signals were read at a 50 Hz sample rate, converted to coefficient form, and fed to the control law. The resulting digital surface deflection commands were sent to the servo actuators in the wind-tunnel model through the D-Six I/O module [6]. Results of executing the trim algorithm while translating to a formation position are presented in Figure 5.

Models

Several different aircraft configurations were tested in order to develop an understanding of formation effects, including the following:

Test Entry	Lead Vehicle	Trail Vehicle
Phase I	Wing-Body Configuration	Military Fighter Configuration
Phase II #1	Military Fighter Configuration	Military Fighter Configuration
Phase II #2	Delta Wing Configuration	Delta Wing Configuration
Phase II #2	Small Transport Configuration	Delta Wing Configuration

Each combination represents an aspect of the various applications of this type of testing. The Wing-Body / Military Fighter Configuration (MFC) was used to develop new test techniques and test hardware. The MFC and Delta Wing Configuration (DWC) formations were to investigate regions of maximum performance benefits for improved mission effectiveness for both inhabited and uninhabited vehicles. Views of each of these combinations can be seen in Figures 6 and 7. The DWC / Small Transport Configuration (STC) formation was to study issues related to automated re-fueling of UAVs. This combination can be seen in Figure 8.

Test Results

Throughout testing, the tail vehicle was mounted on the main model support and the lead vehicle was mounted on the carriage rig. To change formation positions, the carriage was moved relative to the trail vehicle. Although there is an influence on the lead vehicle, the most significant effects are those on the trail vehicle. The data presented here is for the trail vehicle and formation positions are relative to the lead vehicle. For clarity, formation positions were non-dimensionalized using the half-span of the lead vehicle. Figure 9 contains a diagram illustrating formation position sign conventions. Not shown is the change in the Z direction, which is positive when the trail vehicle is positioned above the centerline of the lead vehicle.

From the data collected during the tests, increments of lift, drag, pitching moment, side force, rolling moment, and yawing moment were computed for each of the vehicles in formation by removing the baseline, "clean-air" out-of formation effect from respective "dirty-air" in-formation data. These increments revealed the effects of close formation flight on the aerodynamics of both the leader and trail vehicles. A brief discussion of formation effects and is presented below.

Lift, Drag, and Pitching Moment

The contour plots contained in Figures 10 and 11 provide an excellent illustration of the correlation of the forces and moments influencing the trail aircraft with trail aircraft position. The data in Figure 10 is for a MFC model in trail behind a wing-body model. The data in Figure 11 is for a DWC model in trail behind another DWC model. For both formations, the lead vehicle was set at a higher angle-of-attack than the trail vehicle.

The data for both vehicle combinations reveal increases in lift due to the formation near the 2 semi-span location and vertically in the vicinity of the leader wing plane. Data taken at various lead and trail vehicle angle-of-attack combinations indicated that the effect of increased lift is primarily due to position and lead vehicle angle-of-attack [4].

Figures 10 and 11 also present formation effects on drag for the same conditions defined above. Increased drag was seen in the same regions where the lift also increased. In contrast to the lift results, data taken at various lead and trail vehicle angle-of-attack combinations indicated that the trail vehicle angle-of-attack was the primary effect on trail vehicle drag [4].

The pitching moment variation with position can also be seen for both vehicle combinations. For the trailing MFC, a large region of positive pitching moment change occurred from 1 to 2 semi-spans laterally and from the wing plane vertically to 1 semi-span below the leader. The trailing DWC model showed cells of negative pitching moment change just inboard of the wing tips and cells of positive pitching moment change just outboard of the wing tips which decreased to zero effect beyond 2 semi-

spans. Also present were sharp gradients along the wing tips at 1 semi-span. The difference in this data is due to the different number and orientation of lifting surfaces present in each formation.

Lift-to-Drag Ratio

For each vehicle combination, the maximum increase in L/D occurred in the region 2 semi-spans laterally from the leader centerline and in the leader wing plane (DY=0). For this case, both trail vehicles experienced an L/D increase of 30%. It can also be seen for both vehicle combinations that performance degrades significantly in the region directly behind the lead vehicle and that sharp gradients are present laterally near the leader wing tips.

An examination of data taken at various lead and trail vehicle angle-of-attack combinations revealed that performance benefits are directly related to position and lead vehicle lift. When the lead vehicle was set at a lower angle-of-attack than the trail vehicle, very little performance benefit was observed. Very large percent increases in L/D were seen in cases with the large angle-of-attack differences due to relatively small baseline L/D values.

While the percent change in L/D is useful for determining formation positions likely to yield performance benefits, the actual benefit in trimmed flight cannot be determined without considering the drag contributions of the control surfaces. The actual performance benefit will depend on the total drag at the trimmed lift coefficient and this value does not necessarily correspond to the value measured at the fixed angle-of-attack set during wind tunnel testing. However, the data collected from wind-tunnel tests can be used in a six degree-of-freedom flight simulation to determine the trimmed performance benefit. Figure 12 shows an example of data in a simulation aerodynamics model. The tables are a function of lead angle-of-attack, trail angle-of-attack, and x, y, and z position relative to the leader.

Side Force, Yawing and Rolling Moment

Comparing the lateral-direction forces and moments illustrated in Figures 10 and 11 reveals the geometric differences between the two formations presented. The wake impinging on the vertical tails of the trail MFC model causes larger magnitudes and a vertical asymmetry in side force. When in the leaders wing plane, the side forces works to push the vehicle toward the leader centerline. When slightly below the leader wing plane and in line with the leader wing tips, the side force works to push the trail vehicle away from centerline. The trail DWC, with no vertical surfaces, experiences no asymmetries and sees much smaller changes in side force, with direction of the force corresponding to the sidewash generated by the vortices emanating from the lead delta wing.

The yawing moment data is also presented in Figures 10 and 11. For the trail MFC there are distinct asymmetries at positions below the leader. For the trail DWC, the asymmetries are about the vertical and horizontal centerline of the lead vehicle. However, the yawing moment is relatively small in magnitude for both formations.

The trends and magnitudes of rolling moment changes seen in Figure 10 and 11 are similar for both formation combinations. The direction of the rolling moment directly corresponds to the rotation of the rollup of the leader wing tip vortices. Figure 13 presents the results of a wake survey behind an DWC model in the lead position superimposed on a contour plot of rolling moment change experienced by the trail DWC model. At negative lateral positions, the wing tip vortex rotates in a clock-wise manner and the resulting rolling moment is positive or right wing down. At positive lateral positions, the tip vortex rotates in a counter clock-wise manner and the resulting moment is negative, or left wing down.

Surface pressure plots illustrate the source of the induced rolling moments on the MFC model. Figure 14 contains surface plots of the pressure data collected on the test vehicle for three different span-wise distances along with baseline aircraft (out of formation) data. These plots represent data interpolated for chord-wise and span-wise position from on the top surface of the test aircraft. At this position the outboard wing of the trail aircraft is impinged on by the leader's tip vortex causing asymmetric suction on the top surface of the wing and inducing a rolling moment toward the centerline of the lead configuration.

Overall, the force and moment data reveal that magnitudes of the induced moments and the moment gradients become small near the regions of maximum benefit, thus indicating the feasibility of trimmed flight with maximum L/D benefit. However, depending on the specific formation position, yawing and rolling moments may be uncoordinated. In the case of a vehicle with vertical tails, like the MFC, a control strategy must be employed that distributes control power to coordinate roll and yaw while also attempting to trim side force. For vehicles without vertical control surfaces, the use of roll control only to maintain formation position will lead to higher trim lift coefficient for the trail vehicle and in turn might reduce performance benefits.

Concluding Remarks

It has been demonstrated that tools and test techniques have been developed for measuring formation flight effects experimentally. A variety of data can be obtained to support analysis tasks and simulation effects model generation. This includes static force and moment measurements on both lead and trail vehicles, control deflections required to trim, surface pressures, and wake flow angularity.

Formation wind tunnel testing can be readily used to predict performance benefits, to ascertain the feasibility of maintaining trimmed flight while in formation, and the resulting data can be used to aid in the design of control laws for automated station keeping and in-flight refueling.

References

1. Maskew, B., "Formation Flying Benefits Based on Vortex Lattice Calculations," NASA CR-151974, May 1977.
2. Beukenberg, M. and Hummel, D., "Aerodynamics, Performance, and Control of Airplanes in Formation Flight," ICAS paper 90-5.3.9, 1990.
3. Blake, W.B. and Multhopp, D., "Design, Performance and Modeling Considerations for Close Formation Flight," AIAA-98-43434, August 1998.
4. Gingras, D.R., "Experimental Investigation of a Multi-Aircraft Formation," AIAA 99-3143, June 1999.
5. Description taken from: www.lfst.com
6. Hultberg, R., Gingras, D.R., and Bell, J., "Applications of Simulation During Wind-Tunnel Testing," AIAA-2001-4423, august 2001.
7. Blake, W.B and Gingras, D.R., "Comparison of Predicted and Measured Formation Flight Interference Effects," AIAA 2001-4136, August 2001.

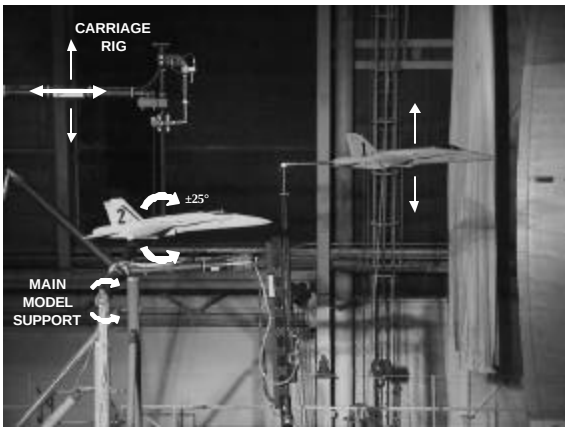

Figure 1. Lead and trail models mounted in the Langley Full-Scale Tunnel.

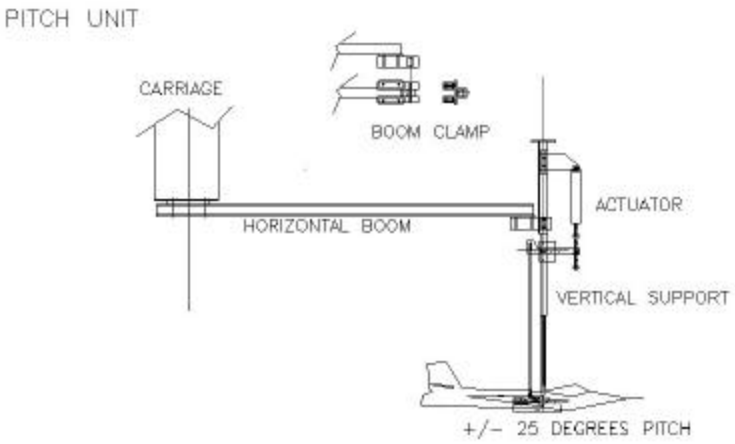

Figure 2. The carriage rig test apparatus.

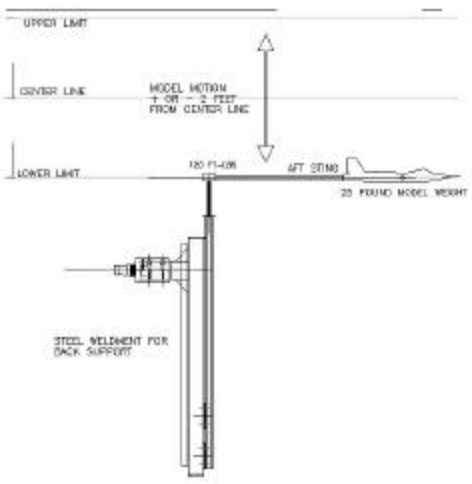

Figure 3. The translation rig mounted on the main model support.

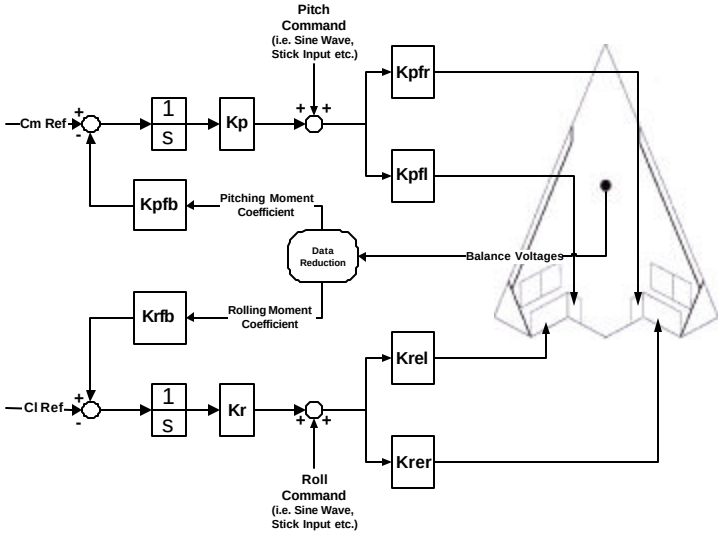

Figure 4. The control law used to trim lead aircraft wake effects.

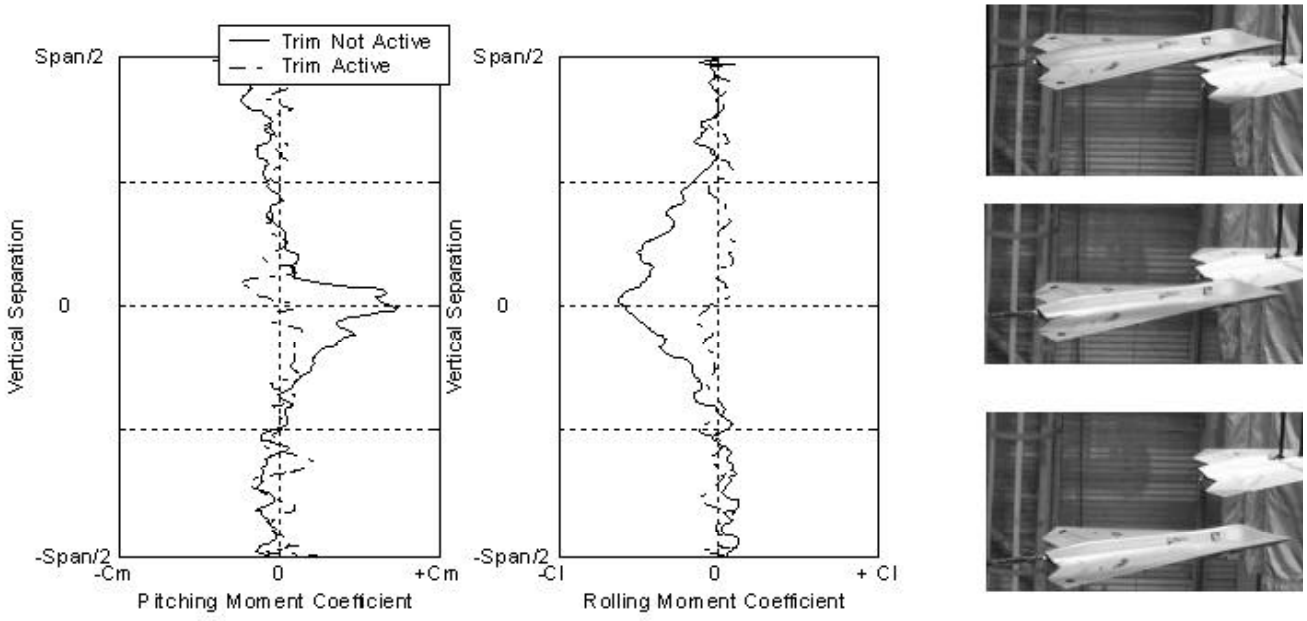

Figure 5. Results of active trimming during dynamic tests.

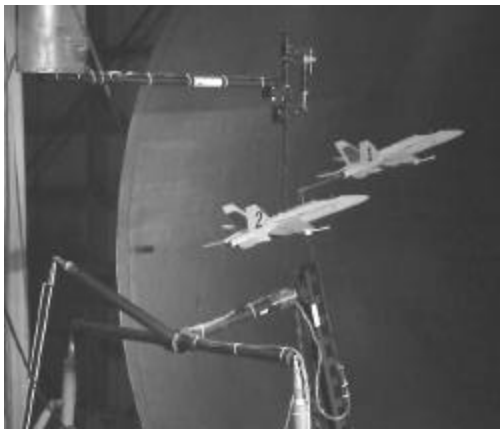

Figure 6. Formation of two F/A-18C aircraft.

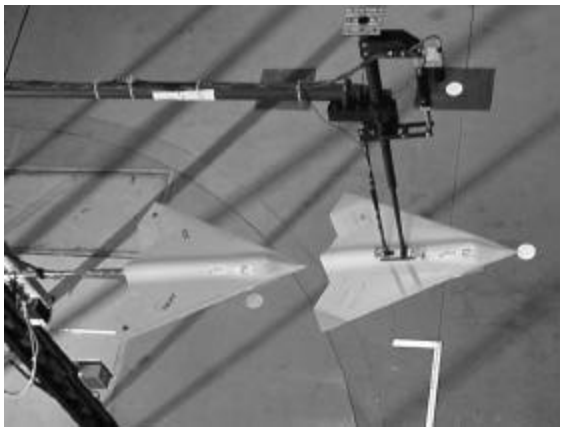

Figure 7. Formation of two ICE 101 aircraft.

Figure 8. Formation of Cessna 210 and ICE 101 aircraft.

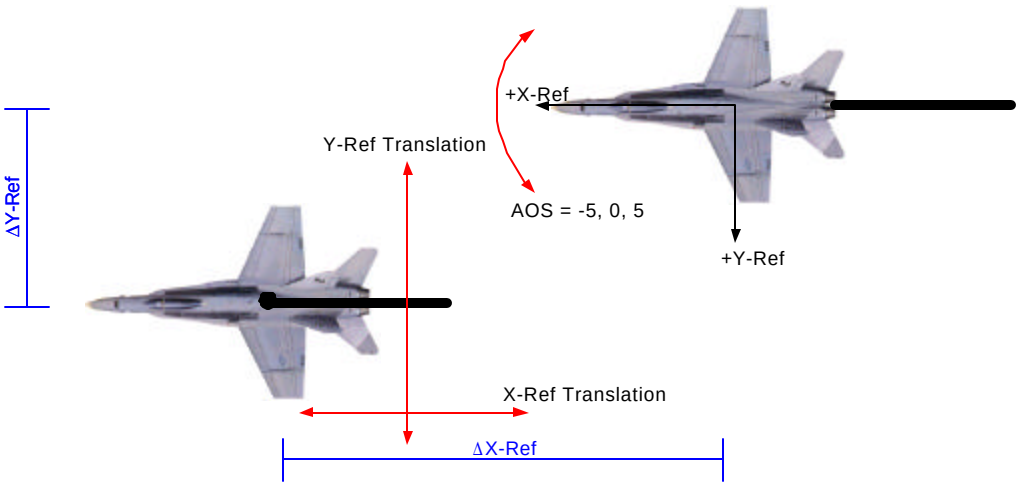

Figure 9. Illustration of formation position sign conventions.

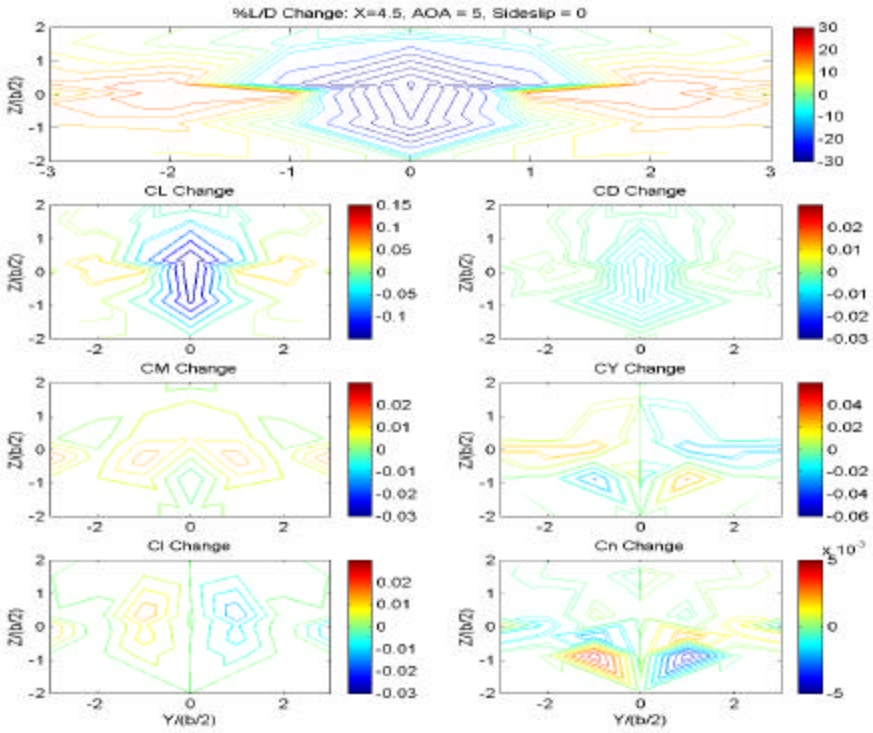

Figure 10. Aerodynamic effects on a military fighter configuration at α =5° and 4.5 semi-spans aft of a lead wing-body model at α =10°.

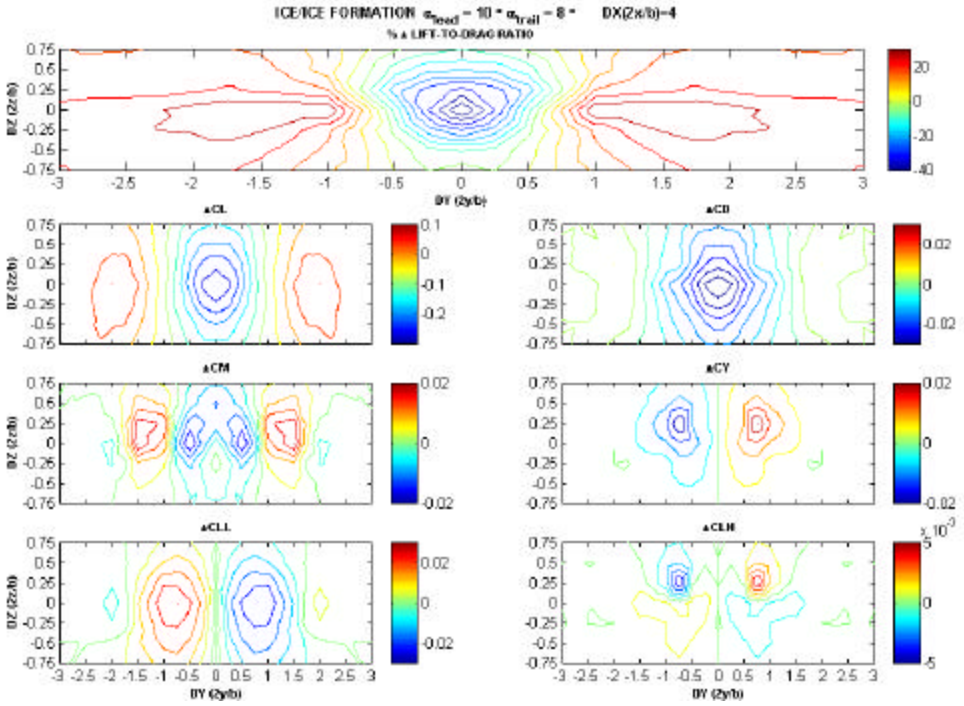

Figure 11. Aerodynamic effects on a delta wing model at α =8° and 4 semi-spans aft of a lead delta wing model at α =10°.

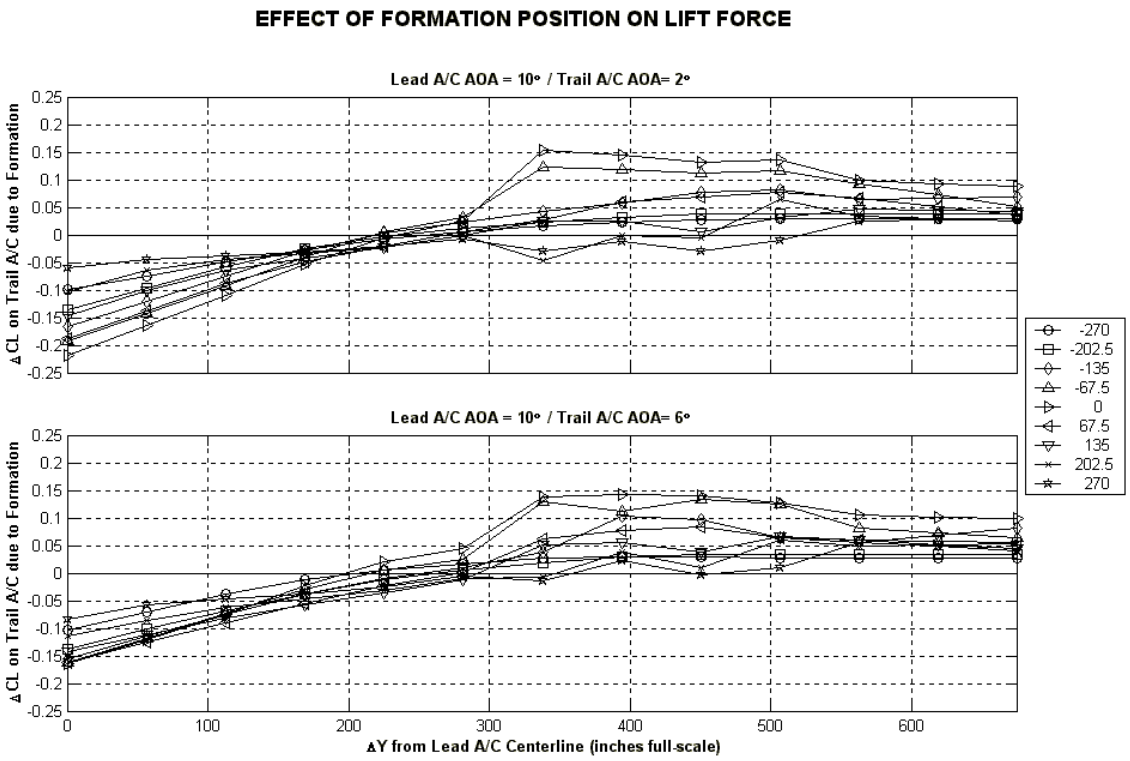

Figure 12. Example of formation effects model data as it wold be represented in simulation data tables.

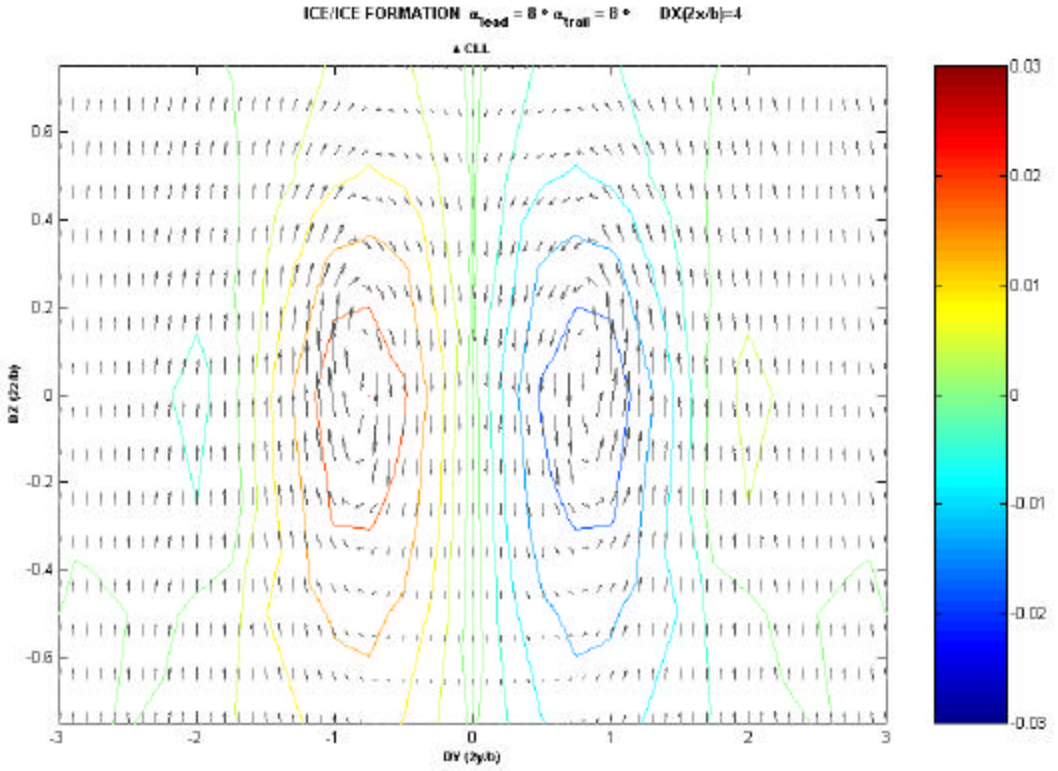

Figure 13. Wake vortices as measured by a five-hole probe correspond to the increment in rolling moment coefficient experienced by the trail aircraft in the formation.

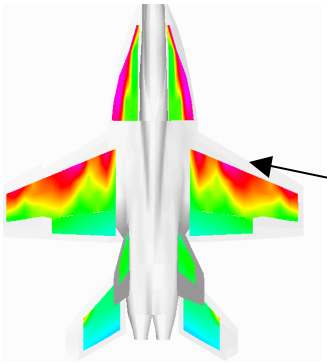

REFERENCE BASELINE (OUT OF FORMATION)

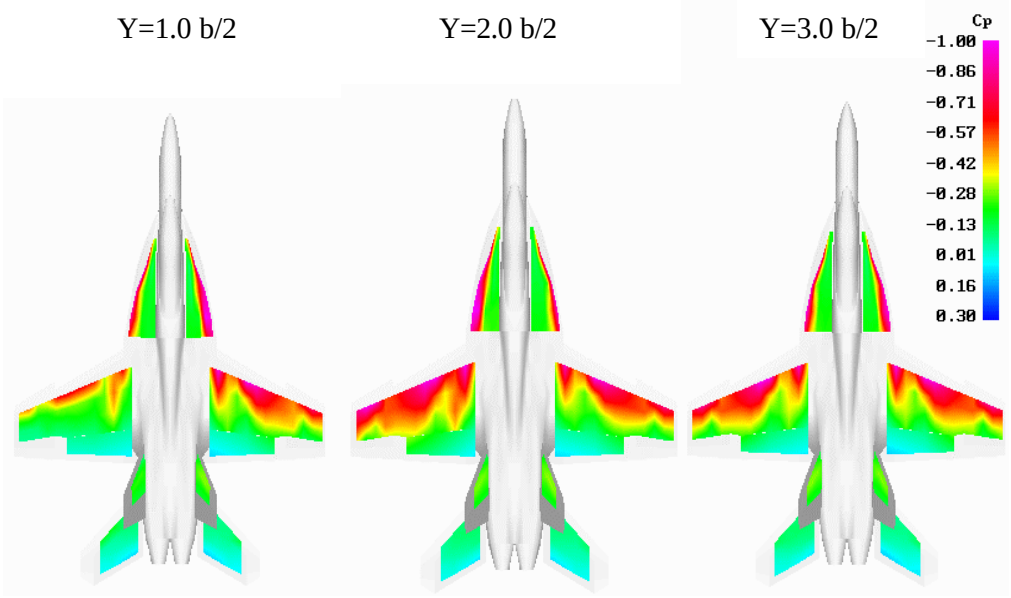

Figure 14. The top-surface pressure distribution of the test aircraft (a = 5° and b = 0°) for three span-wise formation positions) reveals the influence on the wake on the lifting surfaces of the trail vehicle.